these cyclic forcing mechanisms are dominant at periods shorter than ~10 years and longer than a few tens of thousands of years (*19*). The thickness of the beds in Arabia argues against deposition on diurnal or annual time scales. Annual accumulation of more than 10 m of sediment would represent an extremely high deposition rate and would imply that the kilometer-thick deposits accumulated in as little as tens of years. In contrast, deposition at orbital frequencies (~100,000 years) assumes a modest average accumulation rate of ~100 μm per year. This value allows for alternating accumulation and erosion of sediment on shorter time scales, requiring only that the net deposition is roughly constant over long time scales.

Bundling within rhythmic sequences has been a useful indicator of Milankovitch forcing on Earth. In particular, the 5:1 frequency ratio of the precession cycle to the eccentricity cycle for Earth has been observed in the rock record (*19*, *23*). A hierarchy of this type can be used not only to confirm the influence of a periodic forcing mechanism, but also to translate stratigraphic cycles to relative time scales (*24*). At Becquerel crater (Fig. 3), we observed a roughly 10:1 ratio of frequencies over several hundred meters of section, for a total of at least 10 bundles. Individual beds here have a mean thickness of 3.6 ± 1 m, and the bundles are 36 ± 9 m thick. Strata are less distinct near the bottom of each bundle, making it difficult to obtain a precise count for each cycle.

The obliquity of Mars has the largest effect on the global climate, and is one of the most frequently invoked mechanisms for climate change (*2*, *21*, *25*, *26*). The tilt of the planet's spin axis ranges over tens of degrees and can have a strong effect on climate, changing the mean annual insolation even at low latitudes by 10% or more, and affecting the global distribution of volatiles. Among the leading effects, polar condensation of carbon dioxide is expected to reduce atmospheric pressure at low obliquity (*27*). For an aeolian depositional scenario, reduced pressure limits the capacity of the atmosphere to transport sediment (*28*). The obliquity of Mars oscillates with a period of ~120,000 years and is modulated on a time scale of ~1.2 and ~2.4 million years (*29*, *30*). Orbital calculations show that this modulation is expressed more strongly at 2.4 million years for the recent history of Mars, although the ancient history is unknown because of the chaotic nature of the obliquity over long time scales (*31*). As the absolute frequencies of these orbital cycles will not vary greatly over geologic time scales (*30*), this 10:1 ratio in the obliquity cycle is a potential candidate for orbital forcing of the cyclic stratigraphy measured at Becquerel crater. This would imply a formation of one bed per 120,000-year obliquity cycle, one bundle per 1.2-million-year modulation cycle, and deposition of the entire measured section over roughly 12 million years.

The identification of quasi-periodic signals within these layered terrains provides a possible relative chronometer within the martian rock record. Orbital variations stand out as a possible driver of the observed quasi-periodicity, although definitive identification of the cycles involved will require additional information. Likewise, whereas an aeolian scenario provides a clear link to orbital forcing, the specific formation model remains uncertain. Determination of formation time scales ultimately provides a calibration for interpreting the geological history of Mars. With the tentative but reasonable assumption that some water was required to lithify the Arabia deposits, the suggestion of orbital cyclicity implies that a hydrologic cycle may have been active at least intermittently over millions of years. In contrast to the catastrophic surface conditions inferred from impact craters and outflow channels, this strong cyclicity observed in the martian rock record depicts a fundamentally more predictable and regular environment in the ancient past.

References and Notes

1. M. C. Malin, K. S. Edgett, *Science* **290**, 1927 (2000).
2. P. R. Christensen, H. J. Moore, in *Mars*, H. H. Kieffer, B. M. Jakosky, C. W. Snyder, M. S. Matthews, Eds. (Univ. of Arizona Press, Tucson, AZ, 1992), pp. 686–729.
3. A. S. McEwen *et al.*, *J. Geophys. Res.* **112**, E05S02 (2007).
4. J. Laskar, B. Levrard, J. F. Mustard, *Nature* **419**, 375 (2002).
5. S. M. Milkovich, J. W. Head, *J. Geophys. Res.* **110**, E01005 (2005).
6. K. Edgett, *J. Geophys. Res.* **107**, 5038 (2002).
7. M. H. Carr, F. C. Chuang, *J. Geophys. Res.* **102**, 9145 (1997).
8. B. M. Hynek, R. J. Phillips, *Geology* **31**, 757 (2003).
9. R. L. Kirk *et al.*, *J. Geophys. Res.* **113**, E00A24 (2008).
10. By comparing the data to ideal distributions via the Kolmogorov-Smirnov test, the hypothesis that the bed thicknesses were drawn from an exponential distribution can be rejected for four out of five data sets at a 95% confidence level. For a power-law distribution, the null hypothesis can be similarly rejected for all of the data sets. In contrast, a normal distribution is consistent with all of the data sets using this test.
11. M. E. Mann, J. M. Lees, *Clim. Change* **33**, 409 (1996).
12. K. S. Edgett, M. C. Malin, *Geophys. Res. Lett.* **29**, 2179 (2002).
13. J. Waitt, R. B. *J. Geol.* **88**, 653 (1980).
14. G. A. Landis, P. P. Jenkins, *J. Geophys. Res.* **105**, 1855 (2000).
15. B. H. Wilkinson, N. W. Diedrich, C. N. Drummond, E. D. Rothman, *Bull. Geol. Soc. Am.* **110**, 1075 (1998).
16. J. Carlson, J. Grotzinger, *Sedimentology* **48**, 1331 (2001).
17. B. D. Malamud, D. L. Turcotte, *J. Hydrol.* **322**, 168 (2006).
18. A. G. Fischer, *Annu. Rev. Earth Planet. Sci.* **14**, 351 (1986).
19. M. R. House, in *Orbital Forcing Timescales and Cyclostratigraphy*, M. R. House, A. S. Gale, Eds. (Geological Society of London, London, 1995), pp. 1–18.
20. G. Weedon, *Time-Series Analysis and Cyclostratigraphy: Examining Stratigraphic Records of Environmental Cycles* (Cambridge Univ. Press, Cambridge, 2003).
21. H. H. Kieffer, A. P. Zent, in *Mars*, H. H. Kieffer, B. M. Jakosky, C. W. Snyder, M. S. Matthews, Eds. (Univ. of Arizona Press, Tucson, AZ, 1992), pp. 1180–1218.
22. R. Kahn, T. Martin, R. Zurek, S. Lee, in *Mars*, H. H. Kieffer, B. M. Jakosky, C. W. Snyder, M. S. Matthews, Eds. (Univ. of Arizona Press, Tucson, AZ, 1992), p. 1017–1053.
23. W. Schwarzacher, *Earth Sci. Rev.* **50**, 51 (2000).
24. L. A. Hinnov, *Annu. Rev. Earth Planet. Sci.* **28**, 419 (2000).
25. W. R. Ward, B. C. Murray, M. C. Malin, *J. Geophys. Res.* **79**, 3387 (1974).
26. J. W. Head, J. F. Mustard, M. A. Kreslavsky, R. E. Milliken, D. R. Marchant, *Nature* **426**, 797 (2003).
27. F. P. Fanale, J. R. Salvail, *Icarus* **111**, 305 (1994).
28. J. A. Cutts, B. H. Lewis, *Icarus* **50**, 216 (1982).
29. W. R. Ward, in *Mars*, H. H. Kieffer, B. M. Jakosky, C. W. Snyder, M. S. Matthews, Eds. (Univ. of Arizona Press, Tucson, AZ, 1992), pp. 298–320.
30. J. Laskar *et al.*, *Icarus* **170**, 343 (2004).
31. J. Touma, J. Wisdom, *Science* **259**, 1294 (1993).

32. Supported by NASA's Mars Data Analysis Program and by the NASA Earth and Space Science Fellowship program. We thank two anonymous reviewers for helpful comments and suggestions.

Supporting Online Material

www.sciencemag.org/cgi/content/full/322/5907/PAGE/DC1
Tables S1 to S6

16 June 2008; accepted 10 November 2008
10.1126/science.1161870

Photoexcited CRY2 Interacts with CIB1 to Regulate Transcription and Floral Initiation in *Arabidopsis*

Hongtao Liu, Xuhong Yu, Kunwu Li, John Klejnot, Hongyun Yang, Dominique Lisiero, Chentao Lin*

Cryptochromes (CRY) are photolyase-like blue-light receptors that mediate light responses in plants and animals. How plant cryptochromes act in response to blue light is not well understood. We report here the identification and characterization of the *Arabidopsis* CIB1 (cryptochrome-interacting basic-helix-loop-helix) protein. CIB1 interacts with CRY2 (cryptochrome 2) in a blue light–specific manner in yeast and *Arabidopsis* cells, and it acts together with additional CIB1-related proteins to promote CRY2-dependent floral initiation. CIB1 binds to G box (CACGTG) in vitro with a higher affinity than its interaction with other E-box elements (CANNTG). However, CIB1 stimulates *FT* messenger RNA expression, and it interacts with chromatin DNA of the *FT* gene that possesses various E-box elements except G box. We propose that the blue light–dependent interaction of cryptochrome(s) with CIB1 and CIB1-related proteins represents an early photoreceptor signaling mechanism in plants.

Arabidopsis cryptochromes (CRY) mediate light regulation of cell elongation and photoperiodic flowering (*1*, *2*), but the photoactivation mechanism of cryptochrome remains unclear. It has been hypothesized that, similar to other photoreceptors, photoexcited cryptochromes may interact with target proteins to regulate gene expression and physiological

responses (*3*–*7*). However, no light-dependent cryptochrome target protein has been reported in plants, impeding a direct test of this hypothesis. We used a yeast two-hybrid assay to screen for proteins that interacted with *Arabidopsis* CRY2 in a blue light–specific manner (*8*). Because cryptochromes contain the same chromophores—flavin adenine dinucleotide (FAD) and methyltetrahydrofolate (MTHF)—as that of yeast DNA photolyase (*9*–*11*), we reasoned that an *Arabidopsis* cryptochrome expressed in yeast cells should bind the native chromophores to undergo light-dependent protein-protein interactions. Four clones identified in our screen encode various lengths of a basic helix-loop-helix (bHLH) protein (At4g34530), which was referred to as cryptochrome-interacting bHLH or CIB1 (fig. S1). CIB1 is a bHLH protein, for which the function has not been reported, but the mRNA expression is known to be moderately responsive to light (*12*). In yeast cells, the full-length CIB1 and the N-terminal domain of CIB1 interacted with CRY2 in blue light but not in red light or darkness, as shown by two different reporter assays (Fig. 1A and fig. S2). For example, yeast cells irradiated with blue light at the fluence rate of 15 μmol m^{-2} s^{-1} showed appreciable reporter [β-galactosidase (β-Gal)] activity after 60 min of irradiation (Fig. 1A, B15), but no β-Gal activity was detected in cells irradiated with red light of 18 μmol m^{-2} s^{-1} for up to 360 min (Fig. 1A, R18). The CRY2-CIB1 interaction requires relatively high fluence rates. For instance, cells irradiated with 100 μmol m^{-2} s^{-1} blue light showed a CRY2-CIB1 interaction stronger than that in cells irradiated with 15 μmol m^{-2} s^{-1} blue light (Fig. 1A, comparing B100 to B15), whereas little CRY2-CIB1 interaction was detected in cells exposed to 6 μmol m^{-2} s^{-1} blue light for the time tested (Fig. 1A, B6).

We next examined whether the CRY2-CIB1 interaction was dependent on the chromophores of the CRY2 photoreceptor. Because none of the previously isolated *cry2* mutant is known to specifically affect chromophore binding (*2*, *13*), we prepared a site-specific *cry2* mutant, $CRY2^{D387A}$, in which the residue aspartic acid at position 387 was changed to alanine. The residue D387 of *Arabidopsis* CRY2 is part of the FAD-binding pocket conserved in cryptochromes from *Arabidopsis* to human (Fig. 1B and fig. S3) (*14*). In contrast to the wild-type (WT) CRY2 protein, the $CRY2^{D387A}$ mutant protein expressed and purified from insect cells does not contain flavin (Fig. 1C). The flavin-deficient $CRY2^{D387A}$ fusion protein expressed in *Arabidopsis* is "blind" in two blue-light responses: It failed to mediate blue-light inhibition of hypocotyl elongation (Fig. 1D), and it showed no blue light–induced degradation (Fig. 1E). The $CRY2^{D387A}$ mutant protein did not interact with CIB1 in yeast cells (Fig. 1F and fig. S2A). The lack of interaction between $CRY2^{D387A}$ and CIB1 is unlikely due to denaturation of the $CRY2^{D387A}$ mutant protein, because $CRY2^{D387A}$ interacted with constitutive photomorphogenic protein 1 (COP1) in a light-independent manner similar to that shown by the WT CRY2 protein (*15*) (fig. S2E). In addition to flavin, cryptochromes are also known to associate with a folate, MTHF, which acts as the second chromophore (*10*, *16*). However, folate usually disassociates from the apoprotein during purification, and recombinant plant cryptochromes purified from insect cells contain little folate (Fig. 1C) (*11*, *17*, *18*). The folate-deficient CRY2 interacted with CIB1 regardless of light in the in vitro pull-down assays (fig. S2C). It remains unclear whether the lack of light responsiveness of the CRY2-CIB1 interaction in vitro was due to the experimental conditions used or the lack of folate of the purified CRY2.

CIB1 is a nuclear protein that colocalized with CRY2 in the nucleus (fig. S4), and it interacted with CRY2 in plant cells in the BiFC (bimolecular fluorescence complementation) assay (fig. S5). Strong fluorescence was detected in the nuclei of cells cotransfected with C-terminal cyan fluorescent protein (cCFP)–CRY2 and N-

Department of Molecular, Cell, and Developmental Biology, University of California, Los Angeles, CA 90095, USA.

*To whom correspondence should be sent. E-mail: clin@mcdb.ucla.edu

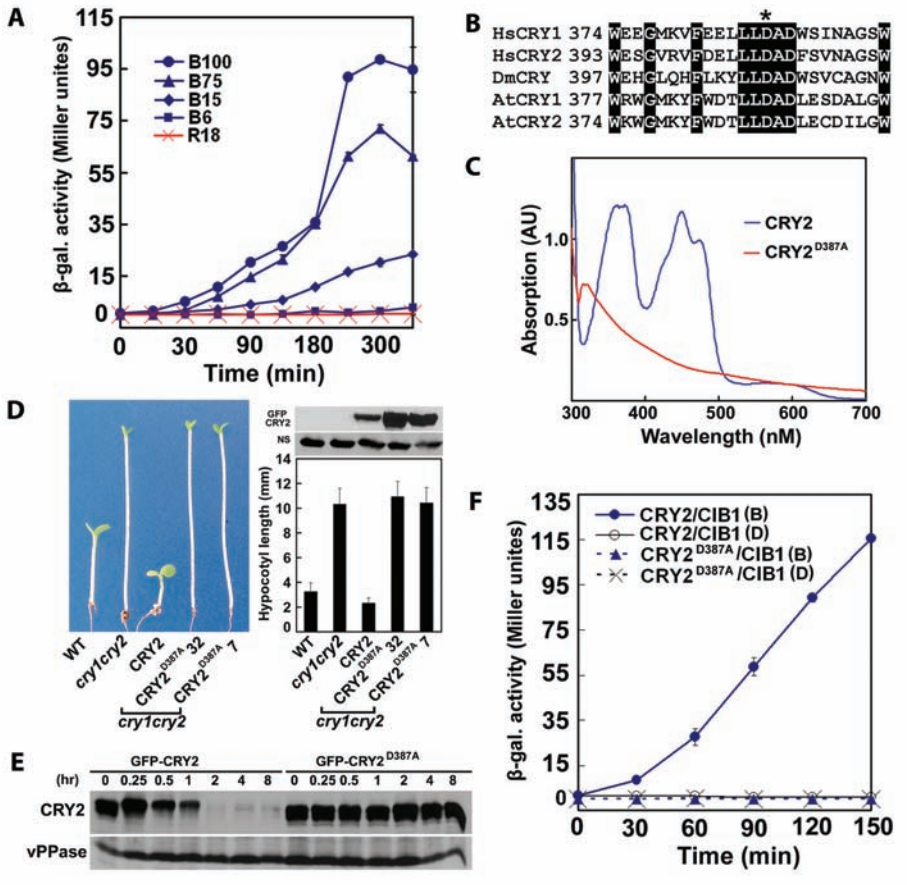

Fig. 1. CRY2 interacts with CIB1 in a blue light–specific and FAD-dependent manner. (**A**) β-Gal assays of yeast cells expressing indicated proteins irradiated with red light (R18, 18 μmol m^{-2} s^{-1}) or blue light (B6 to B100, 6 to 100 μmol m^{-2} s^{-1}) for the durations indicated. (**B**) The FAD-binding pocket of human (Hs), Drosophila (Dm), and *Arabidopsis* (At) cryptochromes. Asterisk indicates D387 of CRY2 and equivalent residues in other CRYs (*34*). (**C**) Absorption spectrum of CRY2 and $CRY2^{D387A}$ mutant proteins. (**D**) A hypocotyl inhibition assay showing the lack of photoreceptor activity of $CRY2^{D387A}$. (Left) Five-day-old seedlings of indicated genotypes grown in blue light (20 μmol m^{-2} s^{-1}). (Upper right) An immunoblot probed with antibody to CRY2 (NS is a loading control). (Lower right) Means of hypocotyl lengths ($n \geq 20$). (**E**) Immunoblot of samples prepared from 5-day-old etiolated seedlings exposed to blue light for the indicated time and probed with antibody to CRY2 and antibody to vacuolar pyrophosphatase (vPPase, the loading control). (**F**) β-Gal assays of yeast cells grown in the dark (D) or irradiated with blue light (B, 30 μmol m^{-2} s^{-1}) for the time indicated.

terminal yellow fluorescent protein (nYFP)–CIB1 plasmids (fig. S5), suggesting reconstitution of the fluorophore upon cCFP-CRY2-nYFP-CIB1 interaction. In contrast, no fluorescence was detected in cells transfected separately with the cCFP-CRY2 or nYFP-CIB1 plasmid (fig. S5). Because of technical difficulties using the BiFC method to study light effects, we examined the CRY2-CIB1 complex formation in plants ex-

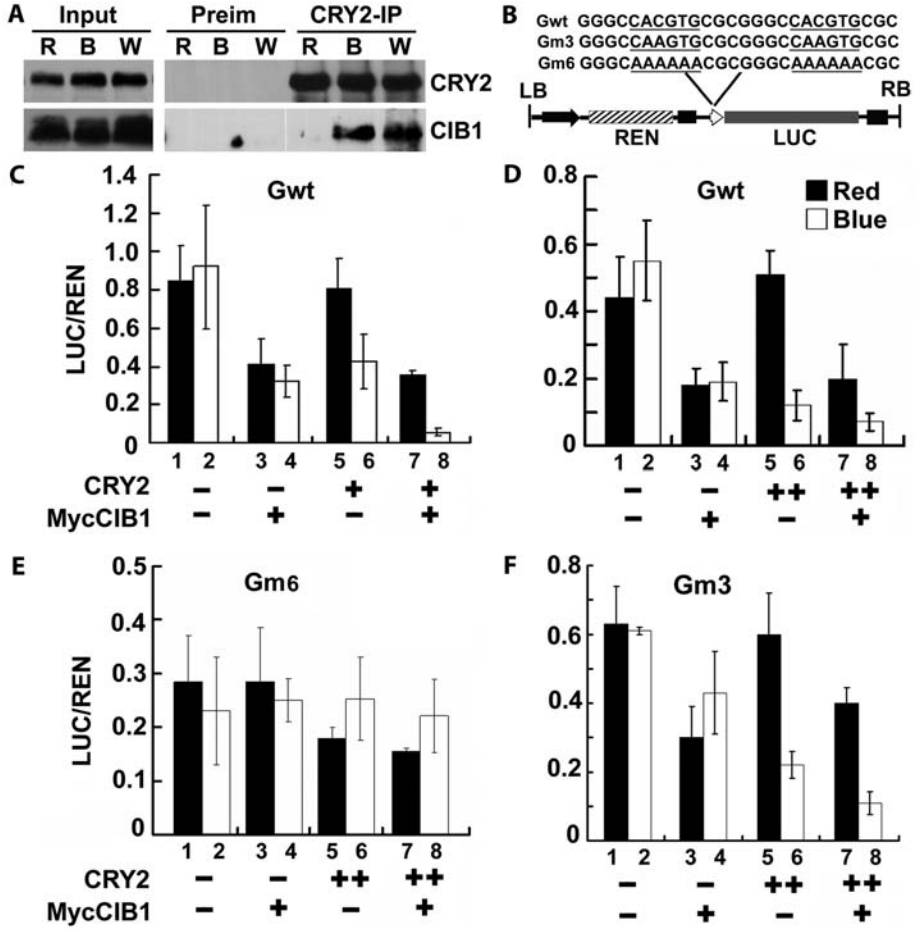

Fig. 2. CIB1 interacts with CRY2 and regulates transcription in plant cells. (**A**) Co-IP assays of samples prepared from 12-day-old *35S::MycCIB1* seedlings grown in continuous red light, pretreated in MG132, then exposed to white light (W), or red light (R), or blue light (B, 20 μmol m^{-2} s^{-1}, 20 min). Total proteins (Input) or IP product of antibody to CRY2 (CRY2-IP) or preimmune serum (Preim) were probed, in immunoblots, by the antibody to CRY2, stripped, and reprobed by the antibody to Myc (MycCIB1). (**B**) Structure of the G-box–driven dual-Luc reporter gene and DNA sequences of the recombinant G-box (Gwt) or mutant promoters (Gm6 and Gmt3). 35S promoter (black arrow), 35S minimum promoter (white arrow head), *Renilla* luciferase (REN), firefly luciferase (LUC), and T-DNA [left border (LB) and right border (RB)] are indicated. (**C** to **F**) Relative reporter activity (LUC/REN) in plants of the indicated genotypes, light condition, and effector (MycCIB1) expression. MycCIB1+, transiently expressed MycCIB1; CRY2+, WT; CRY2-, *cry1cry2* mutant; CRY2++, CRY2 overexpressing in the WT background. Leaves were transfected with the reporter and the effector (MycCIB1), kept in white light for 3 days, transferred to red light for 1 day (Red), and irradiated with blue light (20 μmol m^{-2} s^{-1}) for 2 hours (Blue). The relative LUC activities normalized to the REN activity are shown (LUC/REN, $n = 3$).

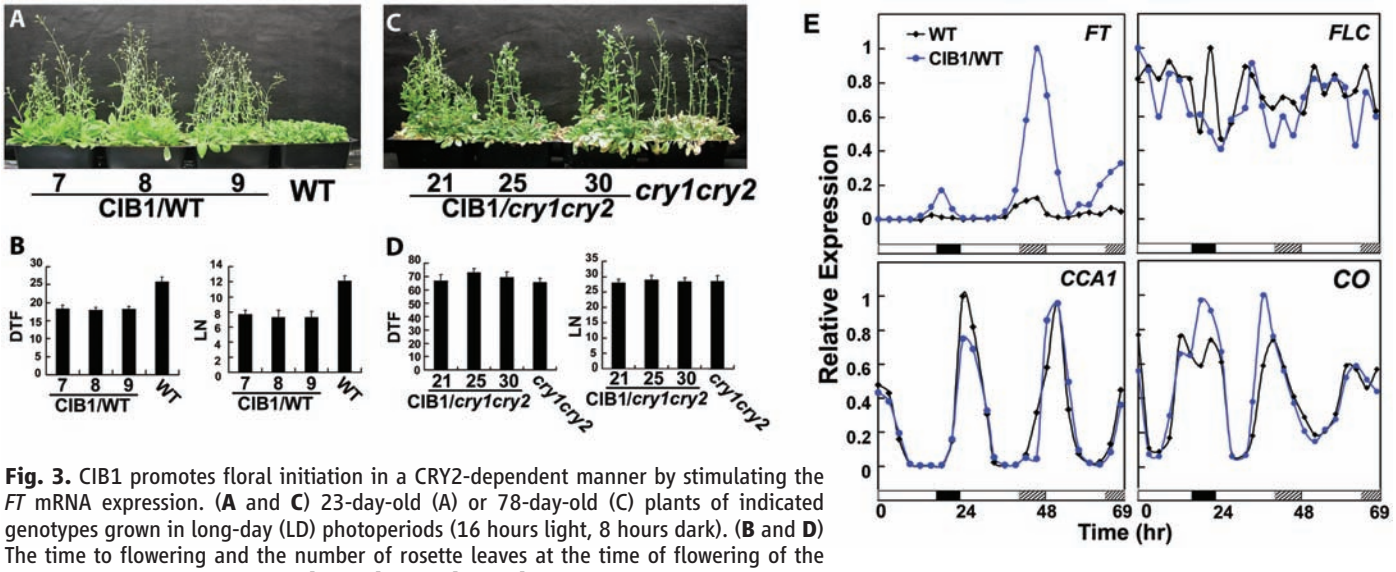

Fig. 3. CIB1 promotes floral initiation in a CRY2-dependent manner by stimulating the *FT* mRNA expression. (**A** and **C**) 23-day-old (A) or 78-day-old (C) plants of indicated genotypes grown in long-day (LD) photoperiods (16 hours light, 8 hours dark). (**B** and **D**) The time to flowering and the number of rosette leaves at the time of flowering of the indicated genotypes shown in A [for (B)] and C [for (D)]. (**E**) Quantitative PCR (qPCR) results showing mRNA expression of the indicated genes in the WT (black diamonds) and transgenic plants overexpressing CIB1 in the WT background (CIB1/WT, blue circles). Plants grown for 6 days under LD photoperiod (light phase, white; dark phase, black) were transferred to continuous white light for 2 days (subjective dark phase, striped). Samples were collected every 3 hours for 1 day in photoperiod and 2 days in continuous light, and the representative results of qPCR are shown.

pressing Myc-tagged CIB1 (MycCIB1/WT), using a coimmunoprecipitation (co-IP) assay designed to detect unstable protein complexes (*8*, *19*. In this experiment, seedlings were pretreated with the proteasome inhibitor MG132 to block blue light–dependent CRY2 degradation (*20*). Samples were then exposed to red light, white light, or blue light (20 μmol m^{-2} s^{-1}) and subjected to co-IP analyses. CIB1 was coprecipitated with CRY2 in samples irradiated with white light (Fig. 2A, W) or blue light (Fig. 2A, B). In contrast, little CIB1 was coprecipitated with CRY2 in samples irradiated with red light (Fig. 2A, R). These results argue strongly that blue light stimulates accumulation of the CRY2-CIB1 complex in plant cells. Taken together, we concluded that CRY2 increases its affinity to CIB1 and CIB1-related proteins in response to blue light.

Like many bHLH proteins, CIB1 interacted in vitro with the highest affinity to an E-box (CACGTG) DNA sequence, which is also known as G box (*21*) (fig. S6). To determine whether CIB1 may act as a transcriptional regulator in vivo, we developed a transient transcription assay in *Arabidopsis* plants (*8*), using a dual luciferase assay (Fig. 2B) (*22*). We examined the effects of Myc-tagged CIB1 (MycCIB1) transiently expressed in plants of different genotypes on the activity of the recombinant G-box promoter under different light conditions (Fig. 2, C to F, and fig. S7). As shown in fig. S7A, both the endogenous CRY2 and transiently expressed MycCIB1 acted as the suppressor of the recombinant G-box promoter in this assay system. The G-box reporter showed MycCIB1- and cryptochrome-independent activities, and MycCIB1 exhibited blue light– and cryptochrome-independent activities (Fig. 2, C and D, and fig. S7A). These observations may be explained by the fact that the activity of the recombinant G-box promoter was affected by multiple photoreceptors and transcription factors in vivo and that CIB1 may have a blue light/cryptochrome-independent effect on transcription. On the other hand, our results also demonstrate that (i) cryptochromes mediate blue-light suppression of the recombinant G-box promoter (Fig. 2, C and D, and fig. S7B, comparing 1/2 to 5/6); (ii) CIB1 possess a blue light– and cryptochrome-dependent activity suppressing the G-box promoter (Fig. 2C and fig. S7B, comparing 3/4 to 7/8, and 5/6 to 7/8); and (iii) the activities of cryptochrome and CIB1 are detected on the reporter promoter containing G box but not on the reporter promoter lacking G box (Fig. 2, comparing 2D and 2E). We concluded that CIB1 is a transcription regulator and that the transcriptional regulatory activity of CIB1 is at least partially dependent on blue light and cryptochromes.

The *cib1* loss-of-function mutant showed no apparent phenotype (fig. S8), which suggests that the function of CIB1 may be redundant to that of other bHLH proteins. To test this hypothesis, we examined seven bHLH proteins related to CIB1, including CIB5, which interacts with both CRY2 and CIB1 (figs. S1 and S8). The *cib1cib5* double mutant showed a mild but statistically significant delay of flowering under the photoperiodic induction condition (*23*, *24*) (fig. S8), which suggests that CIB1 may act to promote floral initiation and that multiple CIB1-related proteins may act redundantly. Consistent with this hypothesis, transgenic plants overexpressing CIB1 in the WT background flowered significantly earlier than the parents in two different light conditions tested (Fig. 3, A and B, and fig. S9). We reasoned that if the function of CIB1 in promoting floral initiation is directly related to its physical interaction with CRY2, this activity of CIB1 should be dependent on CRY2. Indeed, transgenic plants overexpressing CIB1 in the *cry1cry2* mutant background (CIB1/*cry1cry2*) flowered at the same time as the *cry1cry2* parent in both light conditions tested (Fig. 3, C and D, and fig. S9), demonstrating that the function of CIB1 in promoting floral initiation is dependent on CRY2. The different effects of CIB1 overexpression in the two different genetic backgrounds is not due to different levels of CIB1 expression, because CIB1 protein level in none of the three independent CIB1/*cry1cry2* lines tested was lower than that in any of the three independent CIB1/WT lines tested (fig. S9B).

Transgenic plants overexpressing CIB1 exhibited elevated mRNA expression of the flowering-time gene *FT* (Fig. 3E and fig. S10). CIB1 appeared to affect primarily the amplitude, but not the period, of the circadian rhythm of the *FT* mRNA expression (Fig. 3E and fig. S10). CIB1 did not seem to affect mRNA expression of other genes tested, including *CCA1* or *LHY*, which are the clock genes possessing the G-box promoter elements (*7*) (Fig. 3E and fig. S10A). These results indicate that CIB1 may not necessarily tar-

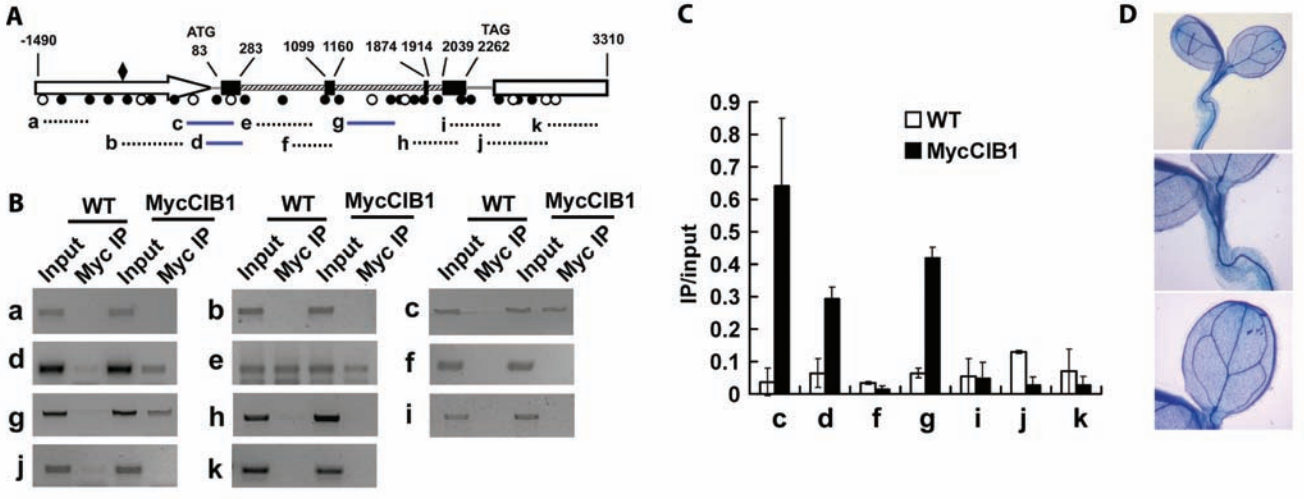

Fig. 4. ChIP-PCR showing interaction of CIB1 and chromatin regions of the *FT* gene. (**A**) A diagram depicting the putative promoter (arrow), 5′UTR (untranslated region) (gray line), exons (black boxes), introns (striped boxes), 3′UTR (gray line), and the putative terminator (white box) of the *FT* gene. Black and white circles indicate positions of E boxes (CANNTG) and 4-nucleotide core of G box (ACGT), respectively. The diamond symbol indicates the position of a CCAAT box. Blue solid lines or black dashed lines depict the DNA regions that were amplified or not amplified by ChIP-PCR using the indicated primer sets, respectively. (**B**) Representative results of the ChIP-PCR assays. Chromatin fragments (~500 base pairs) were prepared from 7-day-old WT seedlings or transgenic seedlings expressing MycCIB1 (MycCIB1/WT), immunoprecipitated by the antibody to Myc, and the precipitated DNA PCR-amplified using the primer pairs indicated. Input, PCR reactions using the samples before immunoprecipitation. (**C**) ChIP-PCR results for the primer pairs that were repeated at least three times were quantified by normalization of the Myc-IP signal with the corresponding input signal (IP/input). The standard deviations ($n \geq 3$) are shown. (**D**) GUS staining of a seedling expressing the CIB1::GUS transgene; different magnifications of the same sample are shown.

get the G-box elements in vivo, although it has the highest affinity to the G-box DNA in vitro. Consistent with this notion, CRY2 and CIB1 exhibited similar effects on a recombinant E-box reporter (Gm3, CAAGTG) as they did on the recombinant G-box reporter in vivo (Fig. 2, comparing D to F), although this E box interacted with CIB1 poorly in vitro (fig. S7). This result suggests that CIB1 may heterodimerize with other proteins, such as CIB5, to interact with E boxes in vivo. We therefore examined whether CIB1 might interact with the *FT* gene that contains various E-box elements, except G box, throughout the genomic DNA (Fig. 4A), using the ChIP-PCR (chromatin immunoprecipitation–polymerase chain reaction) assay. Figure 4, B and C, shows that CIB1 indeed interacted with chromatin fragments associated with the *FT* genomic DNA in vivo. Given that CRY2 control of *FT* transcription took place primarily in the vascular bundle cells (*25*), we also tested whether CIB1 was expressed in those cells. Analyses of the GUS (β-glucuronidase) reporter expression in transgenic plants expressing GUS under control of the CIB1 promoter demonstrated that CIB1 promoter was active in the vascular bundle cells (Fig. 4C). These results support a hypothesis that CIB1 interacts with the E-box regulatory elements of the *FT* gene, whereas CRY2 interacts with CIB1 in response to blue light to affect *FT* transcription and floral initiation.

It has been previously shown that cryptochromes mediate blue-light activation of *FT* mRNA expression by suppressing CO proteolysis (*23*, *24*). The effect of CRY2 on CO protein can be explained by interaction between cryptochromes and the COP1 complex (*15*, *26*, *27*) (fig. S2E), because COP1 acts as an E3 ubiquitin ligase partially responsible for the CO ubiquitination and degradation (*15*, *26*, *27*). On the other hand, our study indicates that CRY2 also functions by interacting with CIB1 to directly affect *FT* transcription. Therefore, cryptochromes may mediate photoperiodic control of floral initiation by at least three different mechanisms: suppression of CO protein degradation (*23*), regulation of light entrainment of the circadian clock (*28*), and direct modulation of *FT* transcription (fig. S11).

Cryptochrome is the only photoreceptor found in all three major evolutionary lineages, from bacteria to plants and animals, although its role as a photoreceptor in mammals remains controversial (*29*–*31*). It has been previously shown that mouse cryptochromes physically interact with two bHLH proteins, CLOCK and BMAL, to suppress their activity on the E-box–dependent transcription (*32*). Given the current hypothesis that cryptochromes evolved independently in different lineages (*29*–*31*, *33*), it remains to be explained how the three-party molecular interaction of CRY, bHLH transcription factors, and E-box DNA elements have evolved in organisms as remotely related as mouse and *Arabidopsis*.

References and Notes

1. M. Ahmad, A. R. Cashmore, *Nature* **366**, 162 (1993).
2. H. Guo, H. Yang, T. C. Mockler, C. Lin, *Science* **279**, 1360 (1998).
3. H.-Q. Yang *et al.*, *Cell* **103**, 815 (2000).
4. X. Yu *et al.*, *Proc. Natl. Acad. Sci. U.S.A.* **104**, 7289 (2007).
5. M. F. Ceriani *et al.*, *Science* **285**, 553 (1999).
6. M. Ni, J. M. Tepperman, P. H. Quail, *Cell* **95**, 657 (1998).
7. J. F. Martinez-Garcia, E. Huq, P. H. Quail, *Science* **288**, 859 (2000).
8. Materials and methods are available as supporting material on *Science* Online.
9. J. L. Johnson *et al.*, *Proc. Natl. Acad. Sci. U.S.A.* **85**, 2046 (1988).
10. K. Malhotra, S. T. Kim, A. Batschauer, L. Dawut, A. Sancar, *Biochemistry* **34**, 6892 (1995).
11. C. Lin *et al.*, *Science* **269**, 968 (1995).
12. L. Ma *et al.*, *Plant Cell* **13**, 2589 (2001).
13. S. El-Din El-Assal, C. Alonso-Blanco, A. J. Peeters, V. Raz, M. Koornneef, *Nat. Genet.* **29**, 435 (2001).
14. C. A. Brautigam *et al.*, *Proc. Natl. Acad. Sci. U.S.A.* **101**, 12142 (2004).
15. H. Wang, L. G. Ma, J. M. Li, H. Y. Zhao, X. W. Deng, *Science* **294**, 154 (2001).
16. S. Ozgur, A. Sancar, *Biochemistry* **42**, 2926 (2003).
17. R. Banerjee *et al.*, *J. Biol. Chem.* **282**, 14916 (2007).
18. J. P. Bouly *et al.*, *J. Biol. Chem.* **282**, 9383 (2007).
19. S. S. Gampala *et al.*, *Dev. Cell* **13**, 177 (2007).
20. X. Yu *et al.*, *Plant Cell* **19**, 3146 (2007).
21. G. Toledo-Ortiz, E. Huq, P. H. Quail, *Plant Cell* **15**, 1749 (2003).
22. R. P. Hellens *et al.*, *Plant Methods* **1**, 13 (2005).
23. F. Valverde *et al.*, *Science* **303**, 1003 (2004).
24. M. J. Yanovsky, S. A. Kay, *Nature* **419**, 308 (2002).
25. M. Endo, N. Mochizuki, T. Suzuki, A. Nagatani, *Plant Cell* **19**, 84 (2007).
26. L. J. Liu *et al.*, *Plant Cell* **20**, 292 (2008).
27. S. Jang *et al.*, *EMBO J.* **27**, 1277 (2008).
28. D. E. Somers, P. F. Devlin, S. A. Kay, *Science* **282**, 1488 (1998).
29. A. R. Cashmore, *Cell* **114**, 537 (2003).
30. C. Lin, D. Shalitin, *Annu. Rev. Plant Biol.* **54**, 469 (2003).
31. A. Sancar, *Chem. Rev.* **103**, 2203 (2003).
32. E. A. Griffin Jr., D. Staknis, C. J. Weitz, *Science* **286**, 768 (1999).
33. T. Todo, *Mutat. Res.* **434**, 89 (1999).
34. Single-letter abbreviations for the amino acid residues are as follows: A, Ala; C, Cys; D, Asp; E, Glu; F, Phe; G, Gly; H, His; I, Ile; K, Lys; L, Leu; M, Met; N, Asn; P, Pro; Q, Gln; R, Arg; S, Ser; T, Thr; V, Val; W, Trp; and Y, Tyr.

35. The authors thank J. Ecker, Z. Wang, W. Laing, S. Poethig, G. Chen, L. Johnson, S. Jacobsen, S. Knowles, E. Tobin, and R. Goldberg for materials and technical assistance. This work is supported in part by NIH (GM56265 to C.L.), University of California–Los Angeles faculty research, and Sol Leshin UCLA-BGU Academic Cooperation programs.

Supporting Online Material

www.sciencemag.org/cgi/content/full/1163927/DC1
Materials and Methods
Figs. S1 to S11
Table S1
References

29 July 2008; accepted 28 October 2008
Published online 6 November 2008
10.1126/science.1163927

A Stress Signaling Pathway in Adipose Tissue Regulates Hepatic Insulin Resistance

Guadalupe Sabio,[1,2] Madhumita Das,[2] Alfonso Mora,[2] Zhiyou Zhang,[3] John Y. Jun,[3,4] Hwi Jin Ko,[3] Tamera Barrett,[2] Jason K. Kim,[3] Roger J. Davis[1,2]*

A high-fat diet causes activation of the regulatory protein c-Jun NH_2-terminal kinase 1 (JNK1) and triggers development of insulin resistance. JNK1 is therefore a potential target for therapeutic treatment of metabolic syndrome. We explored the mechanism of JNK1 signaling by engineering mice in which the *Jnk1* gene was ablated selectively in adipose tissue. JNK1 deficiency in adipose tissue suppressed high-fat diet–induced insulin resistance in the liver. JNK1-dependent secretion of the inflammatory cytokine interleukin-6 by adipose tissue caused increased expression of liver SOCS3, a protein that induces hepatic insulin resistance. Thus, JNK1 activation in adipose tissue can cause insulin resistance in the liver.

Metabolic stress caused by a high-fat diet (HFD) results in activation of the regulatory protein JNK1 (*1*). JNK1 is activated, in part, by increased serum-free fatty acids that induce a stress signaling pathway in target tissues (*2*). JNK1 phosphorylates the adapter protein insulin receptor substrate 1 (IRS1) at an inhibitory site that can block signal transduction by the insulin receptor (*3*). JNK1 may therefore directly induce insulin resistance (*4*). However, JNK1 may also influence insulin sensitivity indirectly. Thus, JNK1 may act in hematopoietic cells to regulate the expression of cytokines that can influence insulin sensitivity (*5*). Indeed, myeloid cells, including macrophages, may be critical (*5*).

To examine the role of JNK1 in myeloid cells during the development of diet-induced insulin resistance, we examined the phenotype of mice with JNK1 deficiency in myeloid cells (figs. S1 and S2) and hematopoietic cells (fig. S3). No significant difference in the response of these JNK1-deficient HFD-fed mice, compared with control HFD-fed mice, was detected in glucose and insulin tolerance tests (figs. S2 and S3). These data indicate that, although JNK1 in hematopoietic cells may contribute to HFD-induced insulin resistance, other cell types must also participate in the development of insulin resistance. Adiposity is known

Photoexcited CRY2 Interacts with CIB1 to Regulate Transcription and Floral Initiation in *Arabidopsis*

Hongtao Liu, Xuhong Yu, Kunwu Li, John Klejnot, Hongyun Yang, Dominique Lisiero, and Chentao Lin

Science, 322 (5907), • DOI: 10.1126/science.1163927